

Article

Electrocatalysts Based on Novel Carbon Forms for the Oxidation of Sulphite

George Pchelarov ^{1,*}, Dzhamal Uzun ¹, Sasho Vassilev ¹, Elena Razkazova-Velkova ², Ognian Dimitrov ¹ , Aleksandar Tsanev ³, Adriana Gigova ¹, Nadezhda Shukova ² and Konstantin Petrov ¹

¹ Institute of Electrochemistry and Energy Systems, Bulgarian Academy of Sciences, G. Bonchev St., Building 10, 1113 Sofia, Bulgaria; dzhamal.uzun@iees.bas.bg (D.U.); sasho.vassilev@iees.bas.bg (S.V.); ognian.dimitrov@iees.bas.bg (O.D.); a.gigova@iees.bas.bg (A.G.); k.petrov@iees.bas.bg (K.P.)

² Institute of Chemical Engineering, Bulgarian Academy of Sciences, G. Bonchev St., Building 103, 1113 Sofia, Bulgaria; razkazova.velkova@gmail.com (E.R.-V.); nastemi1@abv.bg (N.S.)

³ Institute of General and Inorganic Chemistry, Bulgarian Academy of Sciences, G. Bonchev St., Building 11, 1113 Sofia, Bulgaria; tsanev@abv.bg

* Correspondence: g.pchelarov@iees.bas.bg

Abstract: Described herewith is an electrochemical method to decontaminate sulphur compounds. Studies were carried out of sulphites (SO_3^{2-}) oxidation on a range of anode catalysts. The electrocatalysts were characterized by scanning electron microscopy, XRD, XPS and BET. Polarization curves were recorded of electrodes incorporating lyophilized higher fullerenes and manganese oxides. The experiments showed that lyophilized higher fullerenes and $\text{C}_{60}/\text{C}_{70}$ fullerene catalysts in conjunction with manganese oxides electrochemically convert sulphites (SO_3^{2-}) to sulphates (SO_4^{2-}). The oxidation products do not poison the electrodes. The XPS analysis shows that the catalysts incorporating DWCNTs, MWCNTs and higher fullerenes have a higher concentration of sp^3C carbon bonding leading to higher catalytic activity. It is ascertained that higher fullerenes play a major role in the synthesis of more effective catalysts. The electrodes built by incorporating lyophilized catalysts containing higher fullerenes and manganese oxides are shown as most promising in the effective electrochemical decontamination of industrial and natural wastewaters.

Keywords: higher fullerenes; $\text{C}_{60}/\text{C}_{70}$; carbon nanotubes; manganese oxides; electrocatalyst; environment; sulphite decontamination



Citation: Pchelarov, G.; Uzun, D.; Vassilev, S.; Razkazova-Velkova, E.; Dimitrov, O.; Tsanev, A.; Gigova, A.; Shukova, N.; Petrov, K. Electrocatalysts Based on Novel Carbon Forms for the Oxidation of Sulphite. *Catalysts* **2022**, *12*, 93. <https://doi.org/10.3390/catal12010093>

Academic Editor: Vincenzo Baglio

Received: 15 December 2021

Accepted: 11 January 2022

Published: 14 January 2022

Publisher's Note: MDPI stays neutral with regard to jurisdictional claims in published maps and institutional affiliations.



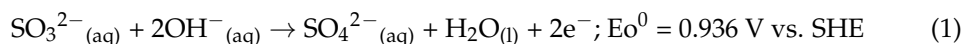
Copyright: © 2022 by the authors. Licensee MDPI, Basel, Switzerland. This article is an open access article distributed under the terms and conditions of the Creative Commons Attribution (CC BY) license (<https://creativecommons.org/licenses/by/4.0/>).

1. Introduction

The aim of our research is to seek out effective novel carbon-based catalysts for the oxidation of hydrogen sulphite at low concentrations. The overall goal is to decontaminate pollutants such as sulphides (H_2S , HS^-) and sulfur dioxide (SO_2) to sulphites (SO_3) and consequently into environmentally friendly compounds such as sulphates (SO_4). This current work is aimed at the investigation of new carbon nanomaterials applicable as catalysts in electrodes intended for use in electrochemical systems to oxidize sulphite. One way to control SO_2 emissions is by flue gas desulphurization, where SO_2 is scrubbed and chemically converted to sulphite (SO_3^{2-}) at a slightly alkaline pH and then electrochemically oxidized to sulphate. This work is part of our efforts to convert the hydrogen sulphide found in Black Sea waters yielding green hydrogen to be applied in fuel cells with relevance as regards the Green Deal.

Sulphate and dithionate are deemed to irreversibly form during the oxidation of sulphite in alkaline solutions [1–3]. Given that the electrolytic oxidation of sodium sulphite to sodium sulphate Na_2SO_4 and to sodium dithionate $\text{Na}_2\text{S}_2\text{O}_6$ are electrolytically irreversible, no diaphragm is needed [4]. Hydrogen is evolved at the cathode during the electrolysis of

alkaline solutions of sulphites (pH > 7), but SO_3^{2-} anions are not reduced [5]. Some of the possible reactions occurring at the anode in alkaline media are presented below [5,6]:



At higher potentials the evolution of oxygen is possible with the wholesome reaction in an alkaline solution being:



The processes of sulphite oxidation on the anode were studied using the following carbon materials: graphite, pyrographite, activated carbon and others [7,8]. The catalytic performance of fullerenes, higher fullerenes and carbon nanotubes is dependent on electronic states and spin characteristics of the carbon system [9]. Sulfate activation is due to electron transfer from the catalyst, in this study fullerenes, higher fullerenes and carbon nanotubes, the abundant flow of electrons in the sp^2 hybridized warped surface of these materials should facilitate electrons detached from the anode, yielding 2OH^- hydroxyl radicals from the water in the electrolyte, thus generating sulfate. The π orbitals of higher fullerenes and carbon nanotubes contain s electrons and also p electrons, which lead to higher chemical activities [10]. In addition, defect sites such as vacancies and five carbon rings, zigzag edges with unconfined π electrons and Lewis basic groups such as ketonic and quinone groups (C=O) at the defect edges of nanocarbons induce a redox process [11–16]. Doping with N atoms promotes the catalytic process due to an increase in the number of electrons available to aid 2OH^- hydroxyl radical synthesis. Nitrogen is more electronegative and has a smaller covalent radius that facilitates electron transfer from adjacent carbon atoms, giving rise to an asymmetric spin and charge density [17,18]. It was suggested that metal-based catalysts can produce both hydroxyl and sulfate radicals [19,20].

Carbon-based electrodes have been widely used in electrochemistry since their development in the fifties [21]. As an element, carbon has the ability to bond covalently with a host of orbital hybridizations. The landmark paper published in 1985 by Kroto, Curl and Smalley unveiled the world of fullerenes, suggesting that these might find application in catalysis, essentially fullerenes and nanotubes are nanoclusters.

Research in the field of N-doped carbons began in the 1980s [22,23]. To date, numerous synthesis approaches have provided support materials able to improve the performance of the transition metal catalyst-support compounds [24–29].

Pyrrole ($\text{C}_4\text{H}_4\text{NH}$) is a five-membered ring first recognized by F. Runge. PolyPyrrole (PPy) is an insulator, but its oxidized derivatives are good electrical conductors. PPy was applied as a catalyst in electrocatalysis [30,31].

A drawback of manganese oxide catalysts is the poor electrical conductivity. The catalytic activity of Mn_3O_4 and MnO_2 can be enhanced by the incorporation of conductive carbon material in conjunction with the bound manganese compounds. The end catalysts are prepared by the addition of Super C 65, Vulcan XC 72, and Kuraray YP 50F via a sol-gel technique employing a MnO_2 precursor.

Based on all these achievements we studied small gap fullerenes also known as higher fullerenes (lattice structure spheres built up by more than 60 carbon atoms); fullerenes $\text{C}_{60}/\text{C}_{70}$; Multi-Wall Carbon Nanotubes (MWCNTs) and Double-Wall Carbon Nanotubes (DWCNTs). Vulcan XC-72 has historically been used as an electrocatalyst support and utilized by us to build up the electrodes [32]. Applied in this study is a method to fabricate the electro-catalyst deposited transition metal—Mn using a lyophilization process [33]. In our experiments, we introduce manganese acetate as the metal source.

2. Results

2.1. XRD Studies

Presented in Figure 1 is the X-ray diffraction pattern of pure PPy. The XRDs scanned in our lab showed that PPy exhibits distinct diffraction peaks at 2θ of 14.52° , 19.08° , 23.08° , 25.82° , while the small gap fullerenes (higher fullerenes) have a multi-peak structure between 19.6° and 20.48° , which were purchased from Sigma Aldrich. The C_{60}/C_{70} fullerenes have three distinct peaks at 2θ of 10.72° , 17.6° and 20.67° and the DWCNTs have peaks at 26.00° , 42.42° and 44.31° . The latter was purchased from SES Research, Huston. The authors [34] claim to have found that the peak shifts towards 26° in 2θ for SWCNTs.

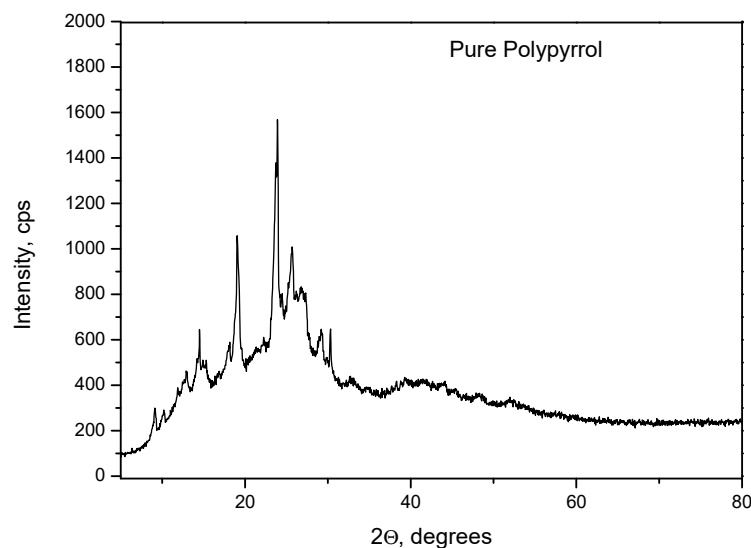


Figure 1. XRD of pure Polypyrrol.

Peaks at 22.00° and 36.92° were ascribed to $\gamma\text{-MnO}_2$, whereas those at 17.94° , 28.78° , 50.00° and 59.00° , respectively, to $\alpha\text{-MnO}_2$ [35]. The XRD of the catalyst synthesized by us from manganese acetate and higher fullerenes exhibits distinct peaks for graphite, $\gamma\text{-MnO}_2$ and $\alpha\text{-MnO}_2$ as shown in Figure 2 [36].

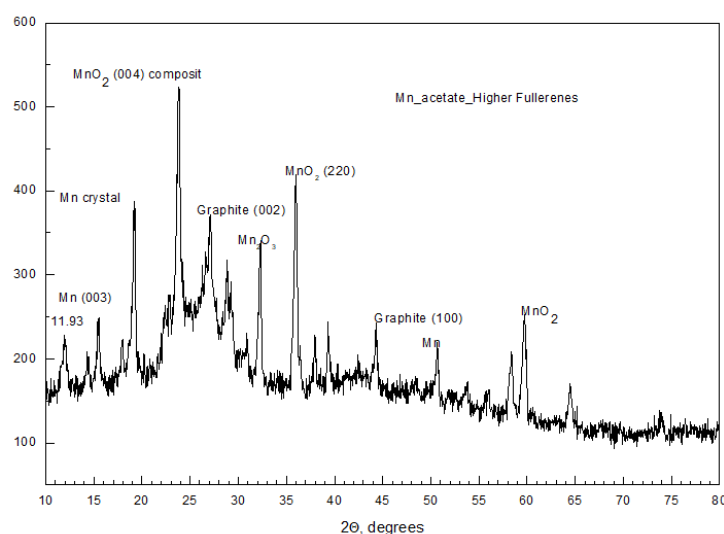


Figure 2. XRD of the catalyst from manganese acetate and higher fullerenes.

2.2. SEM Photographs

Presented in Figure 3a is an SEM picture of the catalyst mass MnAPHF-L that builds up the most catalytically active electrode. Presented in Figure 3b is a SEM picture of

the catalyst MnAPF-L. Shown in Figure 4a is a SEM picture of pristine higher fullerenes. Shown in Figure 4b is a SEM picture of pristine fullerenes C_{60}/C_{70} . It can be seen that the initial structure of both pristine samples consists of large agglomerates with sizes in the micrometer range. The Mn coverage on C_{60}/C_{70} looks more uniform. The pristine C_{60}/C_{70} fullerenes have a porous morphology with fairly large voids while the sample of pristine higher fullerenes has a bulky structure. These surface characteristics change upon the addition of PPy and deposition of manganese oxide. The thermal treatment of the samples (autoclave annealing and freeze-drying) also plays a key role in the formation of a more complex structure. The result is a fine uniform morphology that consists of a porous PPy mesh with small crystals attached to it. The large overall surface area helps boost the catalytic activity of the material.

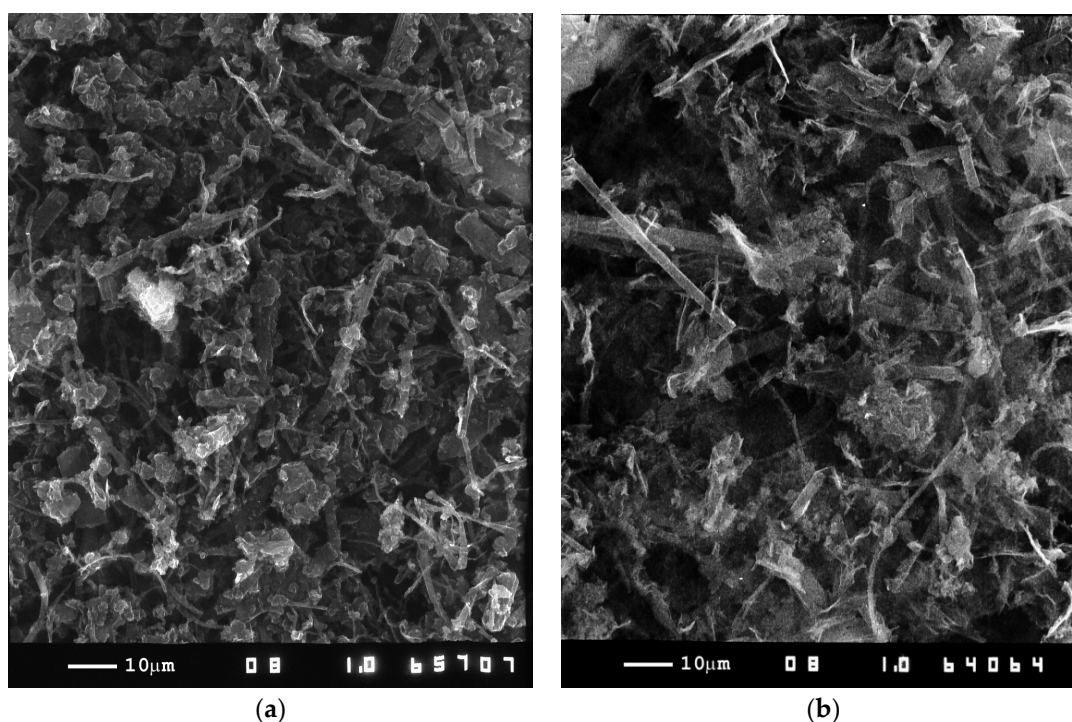


Figure 3. (a) SEM photograph of the catalyst comprised of lyophilized higher fullerenes, PPy and manganese oxides; (b) SEM photograph of the catalyst comprised of lyophilized fullerenes C_{60}/C_{70} , PPy and manganese oxides.

2.3. BET Surface Area and Pore Size Analysis

The specific surface area of our samples MnAP-L, MnAPMWCNTs-NL, MnAPHFDWCNTs-L, was determined (see Table 1) by the Brunauer–Emmett–Teller (BET) method which was developed in 1938 and is applied to isothermal N_2 adsorption measured at 77 K (liquid N_2 temperature) [37]. The structural characteristics were determined and are summarized in Table 1. The isotherm plots of Adsorbed volume cm^3/g versus Relative pressure P/P_0 for Nitrogen in samples MnAP-L, MnAPMWCNTs-NL, MnAPHFDWCNTs-L, are presented in Figure 5a. The measured nitrogen sorption isotherms are close to type III according to the IUPAC classification, with an H3 type hysteresis. Isotherms of this type show that the adsorbate–adsorbent interactions are relatively weak. The steep vertical rise of the isotherms near $P/P_0 = 1$ indicates the presence of macropores in the measured samples.

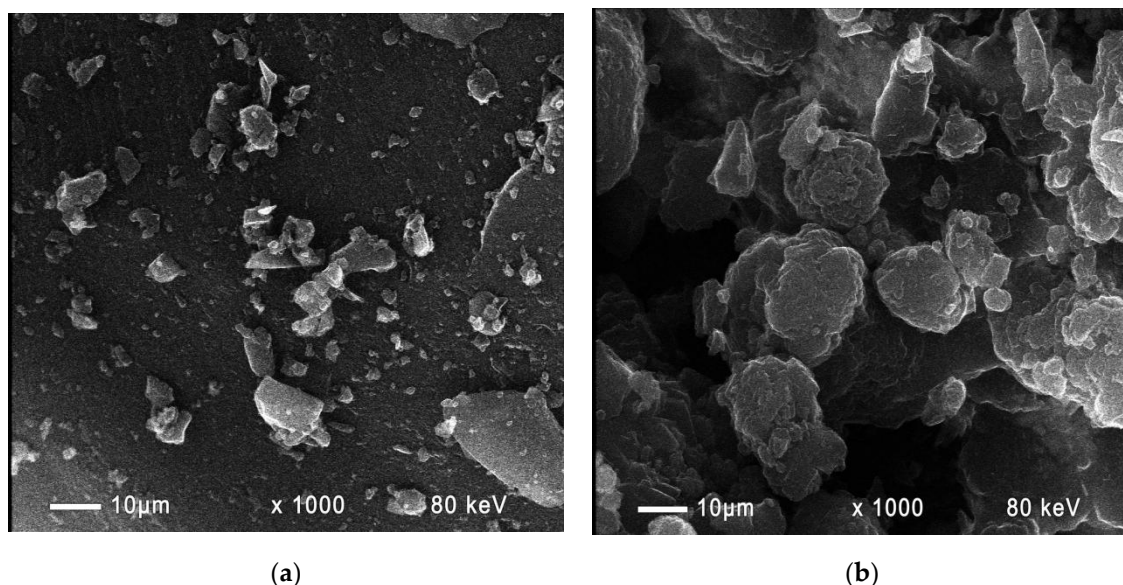


Figure 4. (a) SEM photograph of pristine higher fullerenes; (b) SEM photograph of pristine fullerenes C_{60}/C_{70} .

Table 1. Structural parameters of MnAP-L, MnAPMWCNTs-NL, MnAPHFDWCNTs-L.

Characteristics	MnAPHFDWCNTs-L	MnAP-L	MnAPMWCNTs-NL
Surface Area (BET), m^2/g	17.6	30.1	13.0
Pore Volume, cm^3/g	0.11	0.08	0.07
Pore Diameter (BJH Adsorption), nm	3.1	3.1	3.4
Average Pore Diameter, (4V/S), nm	25.0	10.0	20.0

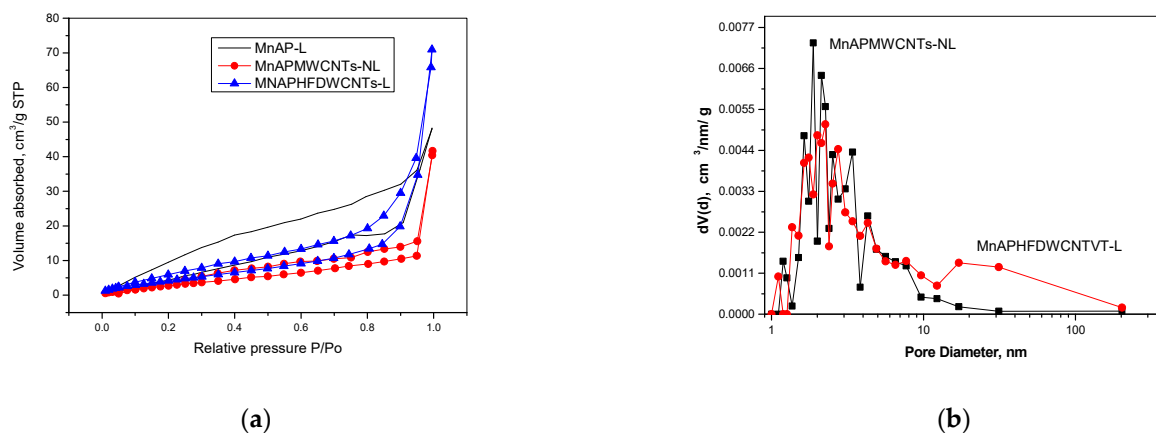


Figure 5. (a) Isotherm plots for samples MnAP-L, MnAPMWCNTs-NL, MnAPHFDWCNTs-L; (b) Pore distribution for samples MnPMWCNTs-NL and MnAPHFDWCNTs-L.

By comparing the measured parameters of the samples studied, we can see that the catalyst MnAP-L has the highest surface area $30 m^2/g$ and the smallest Average Pore Diameter of 10 nm. The pore volume and pore diameter are commensurable for all three materials. The Pore Volume is about $0.1 cm^3/g$ and the Pore Diameter is 3 nm.

2.4. XPS Studies

XPS was used to estimate the composition and the valence state of the chemical elements in the samples. Table 2 shows the chemical composition of the sample surface up to 8 nm in depth.

Table 2. Chemical composition of the sample surface.

Catalysts	C	O	N	Mn
MnAPHFDWCNTs-L	70.8	23.5	3.1	2.7
MnAP-L	74.7	21.7	2.0	1.6
MnAPMWCNTs-NL	74.9	20.4	1.8	2.9

The main component is carbon and its concentration is about 71–75 at.%. The concentration of oxygen is 21–24 at.% that of nitrogen is 2–3 at.% and the concentration of manganese is 2–3 at.%. There are no other contaminants. The reactivity of the fullerenes is defined by the enormous strain engendered by their spherical geometry as reflected in the pyramidalization angles of the carbon atoms. For an sp^2 hybridized (trigonal) carbon atom, planarity implies a pyramidalization angle of $\theta_p = 0^\circ$, whereas an sp^3 hybridized (tetrahedral) carbon atom requires $\theta_p = 19.5^\circ$. The carbon atoms in C_{60} have a $\theta_p = 11.6^\circ$ and it is hence quite obvious that their geometry supports tetrahedral rather than trigonal hybridization. It follows that the chemical conversion of trivalent carbon bonding in C_{60} to tetravalent carbon bonding mitigates the strain at the remaining carbon atoms. Therefore, the reactions that are affected by the carbon atoms are accelerated due to strain relief and this strongly favors fullerene addition chemistry. A fullerene, therefore, just as a perfect single-wall carbon nanotube is without functional groups. However, curvature-induced pyramidalization and misalignment of the π -orbitals of carbon atoms induce a local strain and carbon nanotubes can be expected to be more reactive than flat graphene sheets [38]. Among higher fullerenes, the C_{240} molecule has a $\theta_p \text{ max} = 9.7^\circ$ [39]. The end caps enclosing the DWCNTs and MWCNTs have numerous carbon pentagons with predominant tetrahedral hybridization and hence are quite reactive. Additionally, a differentiation can be expected between the reactivity of carbon nanotubes of different diameters. Sonication in organic solvents produces dangling bonds in CNTs that facilitate further chemical reactions. CNTs have been utilized in reaction chemistry in the past [40]. That is why it is important to identify the functional groups and hybridization state of the carbon atoms in the samples. Presented in Figure 6a are the spectra of deconvoluted C1s core level electrons for samples; MnAPHFDWCNTs-L, MnAP-L and MnAPMWCNTs-NL. The C1s spectra of the sample MnAPHFDWCNTs-L can be divided into four peaks. The second peak, at 284.0 eV is assigned to carbon in the sp^2 hybridization state. We can associate the peak, at 284.8 eV with carbon in the sp^3 hybridization state. The next peak, at 286.2 eV corresponds to carbon with nitrogen bonding characteristic of neutral pyrrolylium nitrogen (N-H), while the C1s core level spectra in sample MnAP-L is deconvoluted entirely according to the deconvolutions of Zhou and coworkers [41] and Chalmers and coworkers [42]. The spectra deconvolute into six peaks. The peaks at 284.1, 285.1 and 286.3 eV correspond to carbon in the sp^2 and sp^3 hybridization state and to carbon bonded to nitrogen as neutral pyrrolylium nitrogen (N-H). The peak at 288.7 eV belongs to defects found in doped PPy.

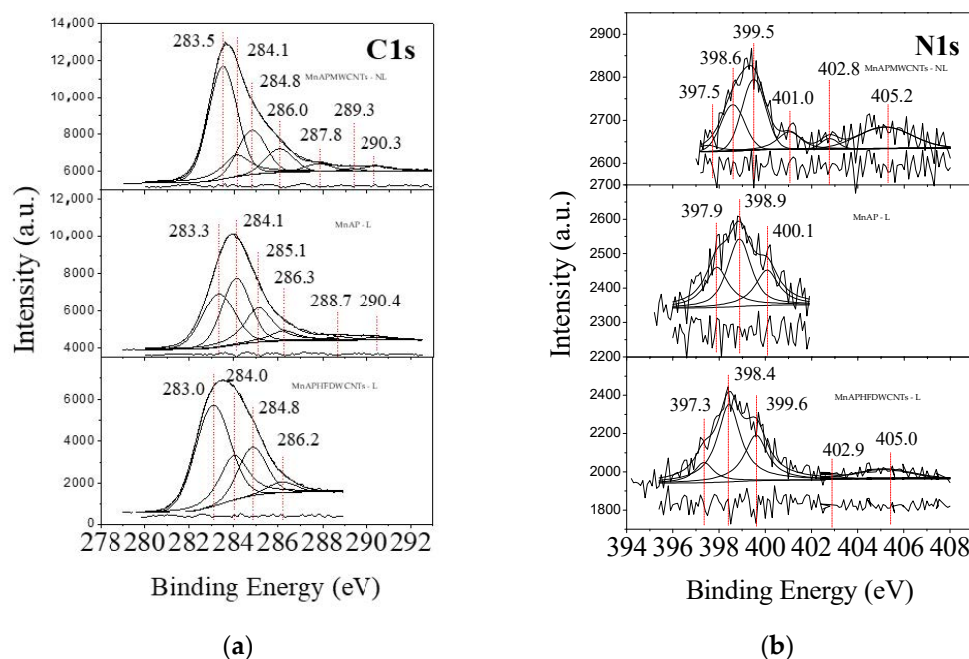


Figure 6. (a) The deconvoluted XPS spectra of C1s core level electrons for samples; MnAPHFDWCNTs-L, MnAP-L and MnAPMWCNTs-NL; (b) The deconvoluted XPS spectra of N1s core level electron signals for samples; MnAPHFDWCNTs-L, MnAP-L and MnAPMWCNTs-NL.

A peak corresponding to a π - π^* shake-up is seen, due to conjugation sp^2 bonding occurring at 290.4 eV. The C1s spectra of sample MnAPMWCNTs-NL is very similar to that of sample MnAPHFDWCNTs-L. There are seven peaks at 283.5 eV, 284.1 eV, 284.8 eV, 286.0 eV, 287.8 eV, 289.3 eV and 290.3 eV. The peaks at 284.1, 284.8 and 286.0 eV are assigned to carbon in the sp^2 and sp^3 hybridization state and to carbon bonded with nitrogen as neutral pyrrolylium nitrogen (N-H). The peak positioned at 287.8 eV is associated with bipolarons ($-C=N^+$) and carbonylic defects (C=O). The peak corresponding to a π - π^* shake-up is seen, again due to conjugated sp^2 bonding occurring at 290.3 eV. The peak positioned at 289.3 eV shows the presence of carbon atoms bound to oxygen through O=C=O bonds [43]. In all C1s spectra, there is a broad peak at 283.0–283.5 eV. This peak is at too low a BE even for the carbide phase as in other authors [44]. However, Ayaka Fujimoto et al. [45] demonstrated that the peak position of sp^3C is basically lower than that of sp^2C using calculations that agree with the results of a few other groups. Insulating diamond was reported to show a wide range of peaks from -1.5 to 3 eV shifted from sp^2C . Thus, charging effects rather than the presence of sp^3C could be one of the actual origins for the conventionally assigned sp^3C peaks of C1s spectra. From the point of view of analyses of general carbon materials with various defects, the increment of FWHM of C1s spectra of carbon materials compared to graphite (sp^2C – sp^2C) could be caused by the presence of electron-withdrawing functional groups, C–H groups, pentagons and heptagons in graphene. These defects can also have other origins of reported sp^3C peaks of carbon materials [45]. MnO_2 groups can also cause such an effect. The positive charging of manganese is increased by the oxygen atoms that bond with it, while the manganese atoms make the carbon surface more positive. This can additionally shift the BE of the peaks in the direction of more BE, i.e., we can assign these peaks to sp^3C bonded to MnO_2 .

As shown in Figure 6b, the deconvolution of N1s signals in the XPS spectrum yields five Gaussian components in samples MnAPHFDWCNTs-L, MnAP-L and MnAPMWCNTs-NL. The low binding energy (BE) component at 397.3–397.5 eV is assigned to the imine nitrogen ($-N=$) [41], the major component at 398.4–398.6 eV is assigned to nitride groups [46] or $-N=$ in cyclic structures [47]. The third peak at 399.5–400.1 eV is associated with neutral N in the PPy ring ($-NH-$) [48]. The peaks at 402.9 eV and 405.2 eV are peaks from $=NH^+$, bipolaron charge carrier species [49] and a peak corresponding to a π - π^* shake up. It indi-

cates the presence of sp^2 bonding [42]. Upon consideration of the literature, the nitrogen signal of doped PPy has only three peaks at about 397.8, 399.7 and 400.5 eV. The present set of peaks of sample MnAP-L are in full agreement with these investigations.

The O1s spectra are shown in Figure 7a. The spectra of all of the samples are broad and they consist of three main peaks. For instance, the deconvolution of sample MnAPHFDWCNTVT-L is shown in the left inset in Figure 7a. The first peak positioned at 529.9 eV is characteristic for the presence of MnO the second peak positioned at 531.3 eV is characteristic for the presence of C=O groups and the peak positioned at 532.6 eV is characteristic for the presence of SO_4^{2-} groups.

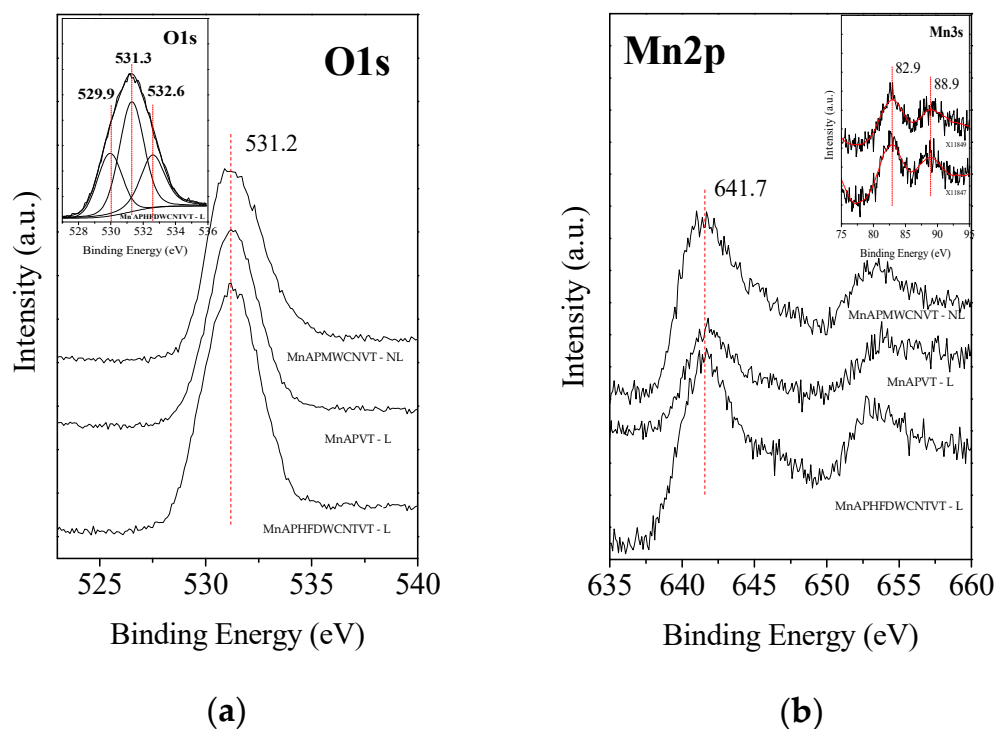


Figure 7. (a) XPS of O1s spectra; (b) XPS of Mn2p and Mn3s (in the inset above-right) for all samples.

The Mn2p core level electron peak is very complex and it has many multiplet-split components, similar to the Cr2p region in chromium oxides [50]. The Mn2p peak has significant split spin-orbit components with Δ metal = 11.2 eV. The BE (641.7 eV) and the presence of a satellite feature that is not present for Mn_2O_3 and MnO_2 show us that we have MnO in the samples. This is confirmed by the Mn3s spectra (Figure 7b, inset above right). However, it is too noisy and that is why we smoothed it to find the peak positions. In it, the distance between the main peak and its satellite feature is 6 eV (Figure 7b, inset above-right) [51].

2.5. Cyclic Voltammetry Studies

While the cyclic voltammograms of electrode MnAPFVT-L are fairly symmetric the cyclic voltammograms of electrode MnAPHFVT-L, which contain higher fullerenes, are asymmetric and are clearly irreversible for the oxidation reactions taking place.

The probable reactions as shown in Figure 8 are:



with peaks for the reduction of Mn as in reaction (4) at around 190 mV and potential plateaus for oxidation/reduction of Mn compounds reaction (5) between 650–800 mV, that correspond to the data as cited in the literature [52]. The insignificant height of the peaks suggests that the catalysts are stable.

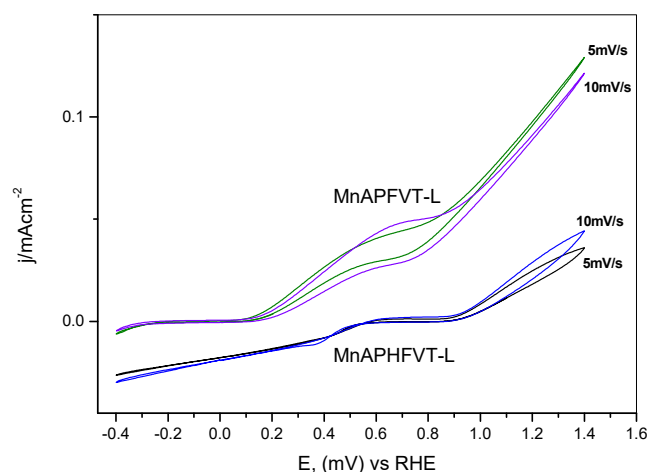


Figure 8. Cyclic voltammograms of the electrodes each containing 7 mg of the catalysts MnAPFVT-L at scan rates of 5 mV/s and 10 mV/s and MnAPHFVT-L at scan rates of 5 mV/s and 10 mV/s at room temperature in 1 M Na₂SO₃ and 18 g/L NaCl, an additive electrolyte.

Shown in Figure 9 is the cyclic voltammogram of the catalyst MnAPFVT-NL. Comparison with lyophilized catalysts (Figure 8) shows that lyophilization leads to stable catalysts.

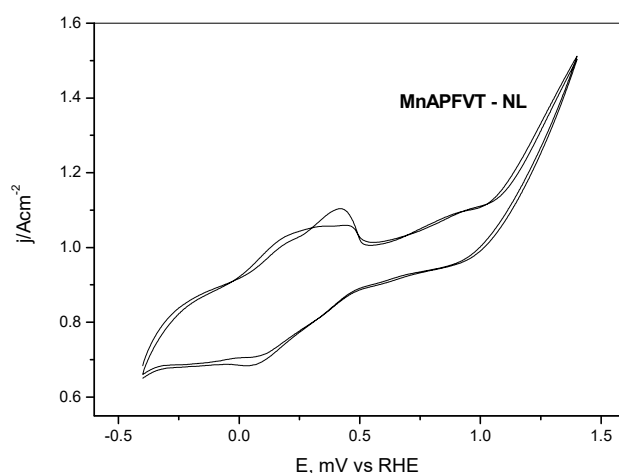


Figure 9. Cyclic voltammograms of the electrode with 20 mg of the catalyst MnAPFVT-NL. The scan rate is 5 mV/s at room temperature in 1 M Na₂SO₃ + 18 g/L NaCl.

2.6. Polarization Curve Analysis

The electrochemical studies include steady-state galvanostatic measurements. The main reactions should be Reactions (1) and (2).

The lyophilized higher fullerene and manganese oxide electrode catalyst sample MnAPHFVT-L was found to be the most effective, yielding the lowest overpotentials at the respective current densities for the polarization curves.

Shown in Figure 10 are the polarization curves of the electrodes prepared from lyophilized and non-lyophilized catalysts. The lowest overpotential is observed in the electrode containing a lyophilized catalyst sample + higher fullerenes + manganese oxides MnAPHFVT-L. With slightly higher overpotentials and inferior characteristics is the electrode containing the most common fullerenes C_{60}/C_{70} + manganese oxides MnAPFVT-L. Additionally shown on this figure are the electrodes built of non-lyophilized catalysts FVT-NL and HFVT-NL, that do not contain manganese oxides. As can be observed the electrode HFVT-NL, which contains higher fullerenes, has better characteristics than electrode FVT-NL, which contains fullerenes C_{60}/C_{70} . The most likely reason for the improved characteristics observed for higher fullerenes as compared to C_{60}/C_{70} quite probably is the greater number of pentagons and hence higher number of sp^3C bonds building up their networks, leading to a higher catalytic activity. The electrolyte is: 1M Na_2SO_3 + 18 g/L NaCl, $T = 20^\circ C$.

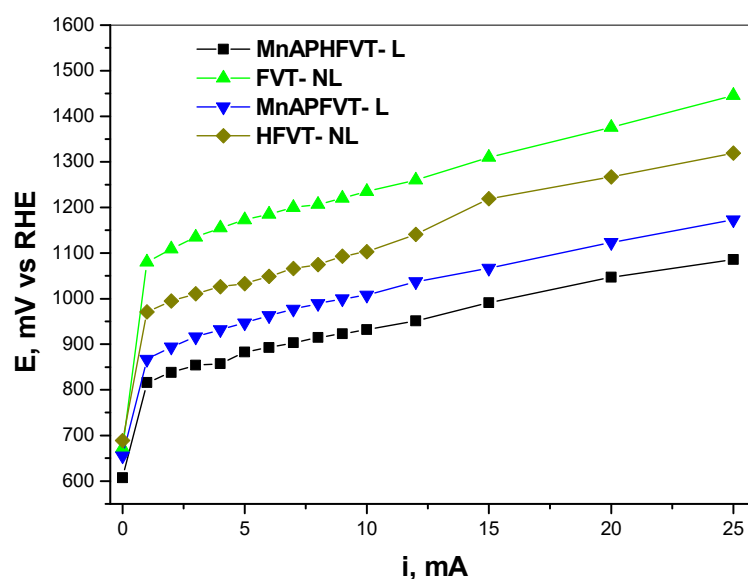


Figure 10. Galvanostatic polarization curves of electrodes prepared from lyophilized (at $-50^\circ C$ and $P = 0.3$ mbar) and non-lyophilized catalysts. Electrolyte: 1M Na_2SO_3 + 18 g/L NaCl, $T = 20^\circ C$.

Shown in Figure 11 are the polarization curves of electrodes prepared from lyophilized catalysts. The lowest overpotentials were observed for the electrode containing higher fullerenes MnAPHFVT-L. With slightly higher overpotentials and therefore with inferior characteristics is the electrode containing the most common fullerenes C_{60}/C_{70} MnAPFVT-L. We assume that the better performance of higher fullerenes is due to the greater number of pentagons and hence the higher number of sp^3C bonds incorporated within their networks, which results in higher catalytic activity. At the same time, the highest overpotentials were observed in the electrodes with NORIT (MnAPNVT-L). Electrolyte: 1 M Na_2SO_3 + 18 g/L NaCl, $T = 20^\circ C$.

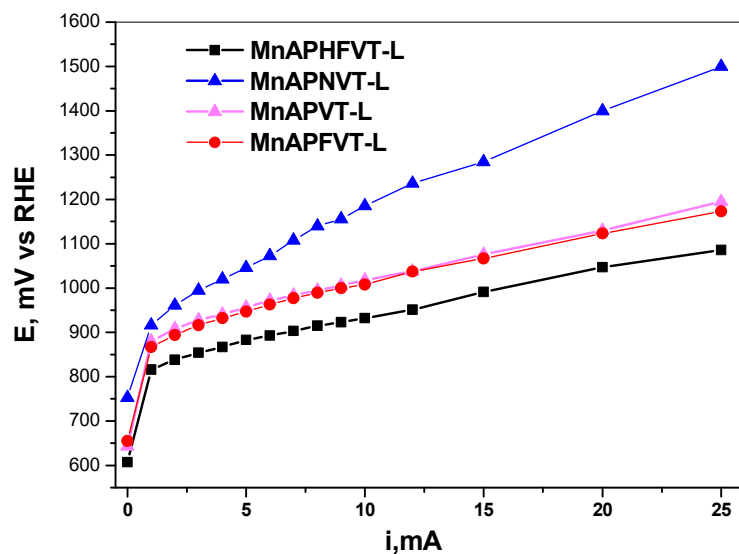


Figure 11. Galvanostatic polarization curves of electrodes prepared from lyophilized catalysts (at $-50\text{ }^{\circ}\text{C}$ and $P = 0.3\text{ mbar}$) (see the table of electrode catalysts by name). Electrolyte: $1\text{M Na}_2\text{SO}_3 + 18\text{ g/L NaCl}$, $T = 20\text{ }^{\circ}\text{C}$.

2.7. Tafel Analysis

As can be observed from the Tafel plots built as shown by Atkins and de Paula [53] in Figure 12 and Table 3, the electrode with lyophilized higher fullerene and manganese inclusion exhibits the highest exchange current density. The next best electrode is the one containing $\text{C}_{60}/\text{C}_{70}$ fullerenes and manganese oxides.

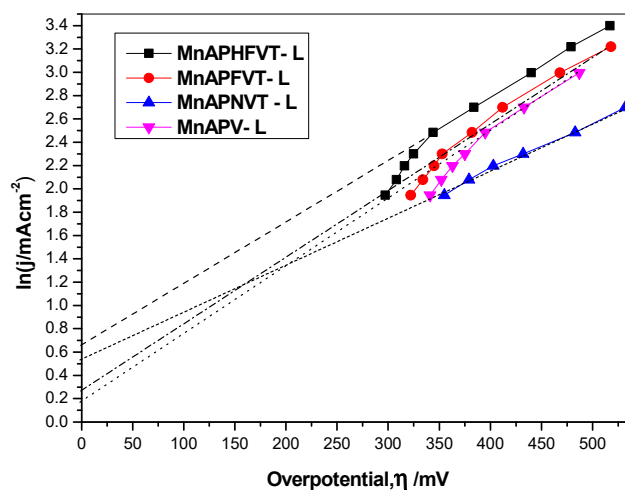
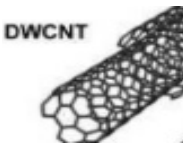
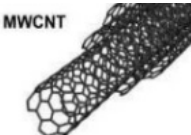


Figure 12. Tafel plots of the electrodes built using the polarization curves shown in Figure 11.

Table 3. Tafel plot values by electrode catalyst name (see Table 4 for the catalyst content by name).

Electrode Catalyst by Name	$\ln j_0$	j_0 [mAcm $^{-2}$]	α
MnAPHFVT-L	0.65	1.916	0.863
MnAPFVT-L	0.265	1.27	0.953
MnAPNVT-L	0.5265	1.69	0.891
MnAPVT-L	0.17	1.19	0.845

Table 4. Electrode catalysts.

Electrode Catalysts by Name		Catalyst Content
L—Lyophilized Catalyst, NL—Non-Lyophilized Catalyst		
MnAPHFVT-L  C n > 70		40 mg manganese acetate, 60 mg polypyrrole, 3 mg Higher Fullerenes
MnAPFVT-L and MnAFPVT-NL  C n = 60, 70		40 mg manganese acetate, 60 mg polypyrrole, 8 mg Fullerenes C ₆₀ /C ₇₀
MnAPNVT-L		40 mg of manganese acetate, 60 mg polypyrrole, 8 mg NORIT
MnAPVT-L		40 mg of manganese acetate, 60 mg polypyrrole
HF-NL  C n > 70		100 mg Higher Fullerenes
F-NL  C n = 60, 70		120 mg Fullerenes C ₆₀ /C ₇₀
MnAPHFDWCNTs-L  C n > 70		23 mg from (7 mg Higher Fullerenes + 20 mg DWCNTs + 20 mg from (40 mg manganese acetate + 60 mg polypyrrole)
MnAPMWCNTs-NL		40 mg manganese acetate + 60 mg polypyrrole + 3 mg MWCNTs

Presented in Table 3 are the electrode catalysts by name listing their respective logarithmic current density; $\ln j_0$, current density; j_0 and α -transfer coefficient values.

From the Tafel plots presented in Figure 12, it can be ascertained that the electrode incorporating the catalyst MnAPHFVT-L and the one built with the catalyst MnAFPVT-L are characterized with a similar mechanism for the electrochemical reactions. The electrodes yielding the highest current densities built incorporating the catalysts MnAPHFVT-L and MnAFPVT-L contain higher fullerenes and fullerenes C₆₀/C₇₀ that have pentagons in their structures. Since the pentagons are more numerous in the higher fullerene structures, it can be expected that these electrodes will yield higher current densities. The electrode incorporating the catalyst MnAFPVT-L with enclosed fullerenes C₆₀/C₇₀ has fewer pentagons than the electrode enclosing higher fullerenes. There are no built-in fullerenes in the electrode MnAPNVT-L so we have to expect even lower values for the measured current densities. This is evident from the Tafel plots presented in Figure 12.

2.8. Dependence of the Anode Potential with Time at a Constant Current Density

In order to verify the effectiveness of the new sulphite oxidation catalysts, electrodes with an area of 10 cm² were built. The technology used was developed at IEES based on

a US patent [54]. A gas diffusion electrode was mounted as the counter electrode. The compound system $\text{Na}_2\text{SO}_3/\text{O}_2$ was employed for this purpose, where the concentration of Na_2SO_3 was monitored following its conversion acting as a fuel in the electrochemical cell as presented in the past [55].

The concentration of sulphite (SO_3^{2-}) was initially determined iodometrically to be 5.3 M and finally found to be 1.8 M after 21 h using starch as an indicator [56]. The production of sulphates is judged both qualitatively by the addition of BaCl_2 (barium chloride) and quantitatively by the residual titration of barium with EDTA [57].

The results show that a conversion of 3.5 M of sulphite (SO_3^{2-}) ions is observed. In our case, we have a conversion of 0.167 M per hour, which is approximately an order higher than the data published in the literature [8]. The differences in the speed of conversion are due to the different initial concentrations.

Heeding the results presented in Figure 13a,b we can conclude that it is possible to build different types of effective electrochemical cells such as the fuel cells: $\text{Na}_2\text{SO}_3/\text{O}_2$; SO_2/O_2 ; SO_3/NO_3 [58] and $\text{Na}_2\text{SO}_3/\text{H}$ [59] based on electrolyzers that can be used to cleanse natural and industrial pollutants while at the same time yielding a surplus of energy.

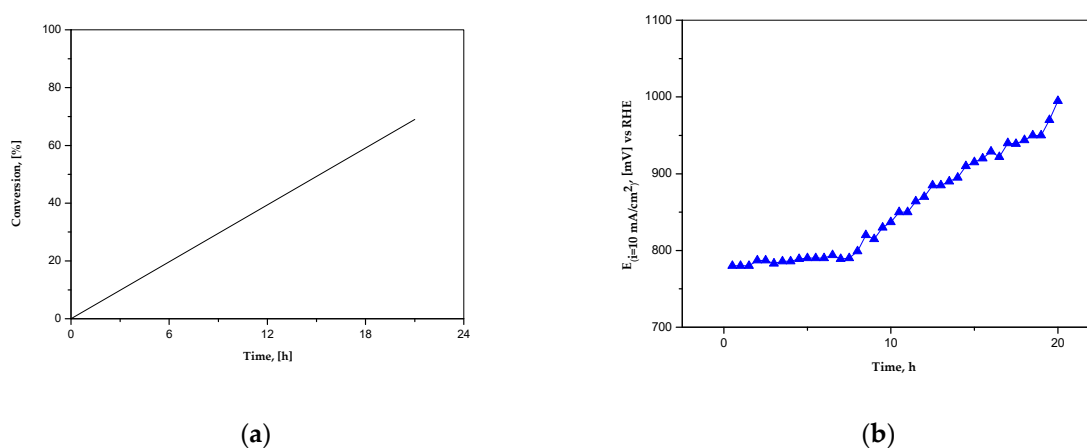


Figure 13. Dependence of the potential with sulphite conversion: (a) percentage of sulphite (SO_3^{2-}) conversion with time, initially standing at 5.3 M with a pH = 10.08 and finally found to be 1.8 M with a pH = 8.07. With an additive electrolyte of 18g/L NaCl; (b) anode (working electrode) potential at constant current density with time. The working electrode was built by covering both sides of a current collector with a catalytic mass of [60 mg (80 mg fullerenes $\text{C}_{60}/\text{C}_{70}$ + 40 mg manganese acetate + 60 mg polypyrrole) + 600 mg (Vulcan XC 72 + 35%Teflon)] with an area of 10 cm^2 . An RHE from Gaskatel was used. The cell volume was 150 mL. The counter electrode was a GDE.

3. Discussion

Essentially, the fullerenes and nanotubes studied are nanoclusters and macro molecules. However, these are rarely found in nature, yet for some time now such nanoclusters have been obtained synthetically in the lab, initially by laser ablation and in consequence utilizing other novel methods. It is important to note that the potential energy signature of a nanocluster is diverse in its complexity. Atomic orbitals (AOs) with the bonding overlaps (δ , & π) in nanoclusters are significant in size. While δ bonding is possible only in nanoclusters formed by transition metals, carbon nanoclusters exhibit σ & π aromaticity. AOs have a greater tendency to hybridize when they are closer in energy and as the $2p-2s$ energy separation in carbon is smaller than in heavier elements, we expect carbon to hybridize more easily. Indeed, the hybridization of AOs in carbon defines organic chemistry as a whole. It is the character of the attained chemical bonding that alters the degree of charge transfer. It appears plausible that aromaticity and covalency occur simultaneously in nanoclusters. In a chemically treated system, the catalytic activity of smaller clusters rises significantly.

Higher fullerenes (HF) are the stable species above C_{60} up to C_{120} . The characteristic of higher fullerenes is that the bonding sites between pentagon atom groups are usually found

to be the most reactive. Because of their high stability with respect to adduct formation and the more positive potentials, higher fullerenes were deemed more promising than C₆₀ as catalysts, even given the fact that their catalytic rate constants are smaller [60]. Nitrogen is incorporated within the catalyst by means of lyophilization and hence these atoms then play a key role as active sites in oxygen reduction [33]. The introduced Nitrogen induces a charge delocalization, thereby changing the chemisorption of O₂ from an end-on adsorption at the surfaces of the CNTs (the Pauling model) to side-on adsorption on to the CNTs found within the electrodes (Yeager model). The adsorption process effectively weakens O–O bonding and leads to reduction at the electrodes with built-in CNTs [61]. The capacity of higher fullerenes to capture O₂ may be utilized to facilitate a more effective oxidation process. The mechanism of electron transfer by fullerenes was studied in the past by density functional-molecular dynamics simulations of the adsorption of oxygen atoms by carbon nanotubes and the interaction between the valence electrons and the ionic cores was assessed with the aid of the pseudopotentials for C and O [62]. An oxygen atom is caught at a fullerene pentagon site where the density of electronic states is higher than at a hexagon site. Modeling the bonding of the carbon atoms showed that, due to the higher density of states at the pentagon sites, these act as electrophilic reaction sites [63]. The pentagons found at the closed cap ends of carbon nanotubes and warped carbon atom surfaces such as higher fullerenes are deemed responsible for a higher density of electronic states leading to increased activation in oxygen reduction.

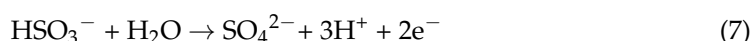
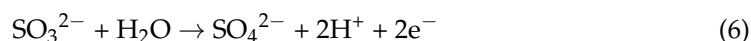
The lyophilized catalysts containing higher fullerenes and DWCNTs are shown to possess the highest activity. XPS analysis confirms that the catalyst incorporating DWCNTs, MWCNTs and higher fullerenes have a high concentration of sp³ carbon bonds and this could well be the reason for the higher activity observed for these materials. The carbon peaks equivalent to sp³ carbon bonding are found in the samples containing a high content of higher fullerenes and DWCNTs. The XPS study ascertained that the lyophilized samples contain a lower concentration of N. At the same time the non-lyophilized catalysts appear to have a larger number of N dangling bonds. Clearly, the process of lyophilization plays a significant role and affects the status of the chemical elements in terms of bonding to other species that make up the surface of the samples. Future work needs to be carried out to unveil the specific nature of carbon and nitrogen bonding within the structures of the fullerenes and nanotubes.

The pristine C₆₀/C₇₀ fullerenes have a porous morphology with fairly large voids while the sample of pristine higher fullerenes has a bulky structure. These surface characteristics change upon the addition of PPy and deposition of manganese oxide. The thermal treatment of the samples (autoclave annealing and freeze-drying) clearly plays a key role in the formation of a more complex structure. The result is a fine uniform morphology that consists of a porous PPy mesh with small crystals attached to it. The large overall surface area helps boost the catalytic activity of the material.

4. Materials and Methods

4.1. Reactions and Experiment

The end reactions of sulphites to sulphates are:



An extensive study of the oxidation states of Sulfur can be found in [64].

The desulphurization reaction via Mn is:



The catalytic properties of a range of anode electrodes were determined with the aid of a three-electrode cell while studying the process of oxidation of sulphites to sulphates

in solution. The solution was 1M Na₂SO₃ + 18 g/L NaCl. The NaCl was an additive electrolyte. The cell volume was 50 mL. The counter electrode was platinum foil. The reference electrode was a “Gaskatel” hydrogen electrode.

The studies of the dependence of the anode potential at constant current density with time were carried out in a cell, with a volume of 150 mL; the counter electrode was a Gas diffusion electrode and the RHE (reference hydrogen electrode) was purchased from Gaskatel. A description of the cell can be found in [55].

4.2. Catalyst Synthesis

The catalysts used by us are listed in Table 4. The process of lyophilization was applied in order to overcome catalyst agglomeration. We used higher fullerenes to maximize the electroactive surface area of the catalyst. A small quantity of higher fullerenes was dispersed in 6 mL of distilled water in a sonic bath for 15 min. Next, (20–40) mg of manganese acetate and (20–100) mg of polypyrrole were slowly added to the aqueous suspension. These ternary components were then baked at 180 °C for 12 h in a Teflon autoclave. Thus, MnO₂ was deposited on the higher fullerene lattice structures with polypyrrole binding. The suspension was finally dehydrated by freeze-drying yielding a complex structure. The higher fullerenes also known as small gap fullerenes were fabricated by Diener and Alford by applying the carbon arc method in a quartz reactor designed for both production and subsequent sublimation, these are commercially available from Sigma Aldrich.

A number of partial polarization curve measurements were made characterizing the incorporated higher fullerenes, deposited MnO₂ and polypyrrole binder in different ratios. The polypyrrole used in the experiments has a conductivity of 10–50 S/cm. An SEM picture of the catalyst MnAPHF-L building up the best electrode is shown in Figure 3 and was synthesized as follows: 3 mg of higher fullerenes were added to 6 mL of distilled water and processed in an ultrasonic bath for 15 min. Between 20 and 40 mg of manganese acetate and 20 to 100 mg of polypyrrole were then slowly added to the water suspension. In consequence, these components were baked at 180 °C for 12 h in a Teflon autoclave. The polarization curve plot of the electrode incorporating the catalyst MnAPHF-L is presented in Figures 11 and 12.

The catalyst MnAPFVT-L building up the second-best electrode as observed by SEM is shown in Figure 3b and was synthesized as follows: 8 mg of C₆₀/C₇₀ fullerenes purchased from SES Research, Huston, Texas were dispersed in distilled water and processed in an ultrasonic bath for 30 min. A total of 40 mg of manganese acetate and 60 mg of polypyrrole were then slowly added to the suspension. The mixture was baked at 180 °C for 23 h in a Teflon autoclave. Thus the particles of manganese oxide were deposited on C₆₀/C₇₀ fullerenes in different ratios. The polarization curve plot of the electrode incorporating the catalyst MnAPFVT-L is presented in Figures 10 and 11.

4.3. Electrode Preparation

Different sample electrodes of the immersed type were prepared by deposition of the sample catalyst on the work surfaces of all electrodes followed by pressing and heating. The electrodes studied have geometrical areas of 1 cm² and 10 cm². The electrodes were prepared from a mixture of the catalyst mass and teflonized carbon Vulcan XC-72 (35% Teflon) as a binder content 60 mg/cm² [55]. The mixture was pressed onto both sides of a stainless steel current collector at 150 °C. Different catalysts were studied: manganese oxides; higher fullerenes; fullerenes C₆₀/C₇₀.

The 10 cm² electrodes were studied by registering the dependence of the anode potential at constant current density with time, while the concentrations (conversion of sulfite) of the electrolyte were determined during the initial and final stage of the experiment with the aid of an analytical method [57].

4.4. Experimental Equipment and Conditions

X-ray diffraction (XRD) patterns were recorded utilizing a Philips diffractometer (Holland) using CuK_α radiation ($\lambda = 1.54178 \text{ \AA}$, 40 kV and 30 mA) with a scanning rate of 2° min^{-1} .

The surface morphology was studied by means of an SEM-JEOL-JEM 200CX (Japan). The images were taken in secondary electrons mode with an accelerating voltage of 80 keV.

BET studies were carried out employing a Quantachrome instrument autosorb iQ acquired from Boynton Beach FL 33426, USA, that measures the quantity of gas adsorbed onto or desorbed from a solid surface at an equilibrium vapor pressure by the static volumetric method.

The XPS studies were performed in a VG Escalab II system, UK, using AlK α radiation with an energy of 1486.6 eV. For the detailed spectra, the analyzer mode was CAE with a pass energy of 20. The chamber pressure was 1.10^{-9} Pa. The Mn2p line of manganese oxide at 641.7 eV was used as the internal standard to calibrate the binding energies. The photoelectron spectra were corrected by subtracting a Shirley-type background and were quantified using the peak area and Scofield's photo-ionization cross-section. The accuracy of the BE measured was ± 0.2 eV.

The 1 cm^2 electrodes were studied by cyclic voltammetry, steady-state polarization curves and Tafel analysis. The cell volume was 50 mL. The cyclic voltammetry measurements were performed with the aid of a Solartron 1286 Electrochemical Analyzer produced at Farnborough, Hampshire, UK. The polarization characteristics were determined by a potentiostat TACUSSELL BIPOTENTIOSTAT type BI-PAD, France. A minimum of three measurements were made for each result to achieve better reproducibility. Arithmetic averages are presented in the graphs.

5. Conclusions

The presented work shows it is possible to oxidize sulphites to sulphates without poisoning (blocking) the electrodes. The results are qualitative and therefore conclusions about the reaction kinetics can not be drawn.

The electrodes prepared with the incorporation of lyophilized catalysts containing higher fullerenes and manganese oxides show reasonable overpotentials that warrant a high catalytic activity capable of oxidizing sulphites to sulphates.

The catalytic masses incorporating DWCNTs, MWCNTs, higher fullerenes and fullerenes have a higher percentage concentration of sp³C carbon bonding, in accordance with the XPS analysis, which could be a reason for the higher activity observed for these catalysts.

The lyophilized catalyst masses containing higher fullerenes and DWCNTs are shown to exhibit the best electrochemical activity.

These novel electrocatalytic masses are found to manifest a reasonable performance in their ability to electrochemically convert sulphite to sulphate.

The catalysts developed are able to decontaminate all the sulphur-based pollutants found in natural and industrial wastewater environments.

Author Contributions: Conceptualization, G.P. and K.P.; methodology, G.P. and D.U.; software, G.P. and D.U.; validation, G.P. and D.U.; formal analysis, G.P., D.U. and K.P.; electrochemical tests, G.P., D.U. and K.P.; XRD, S.V.; SEM, O.D.; XPS, A.T. and G.P.; BET, A.G. and G.P.; chemical analysis, E.R.-V. and N.S.; investigation, G.P., D.U. and K.P.; data curation, G.P. and D.U.; writing—original draft, G.P. and D.U.; writing—review and editing, G.P.; visualization, G.P. and D.U.; supervision, K.P.; project administration, K.P.; funding acquisition, K.P. All authors have read and agreed to the published version of the manuscript.

Funding: The authors kindly acknowledge the financial support of the Bulgarian Ministry of Education and Science under National Research Program EPLUS, approved by DCM No 577 /17.08. 2018 and project № BG05M2OP001-1.002-0014 "Center of competence HITMOBIL—Technologies and systems for generation, storage and consumption of clean energy", funded by Operational Programme "Science and Education For Smart Growth" 2014–2020, co-funded by the EU from European Regional Development Fund.

Acknowledgments: We note with deep gratitude the help of R. Stoyanova from the Institute of Inorganic Chemistry for affording us the opportunity to utilize the institutes' lyophilization and XPS equipment.

Conflicts of Interest: The funders had no role in the design of the study; in the collection, analyses, or interpretation of data; in the writing of the manuscript, or in the decision to publish the results.

References

1. Lewis, G.N.; Randall, M.A. Preliminary study of reversible reactions of sulfur compounds. *J. Am. Chem. Soc.* **1918**, *40*, 356–362. [[CrossRef](#)]
2. Bancroft, W.D.; Magoffin, J.E. Energy Levels in Electro-chemistry. *J. Am. Chem. Soc.* **1935**, *57*, 2561. [[CrossRef](#)]
3. Coursier, J. Interprétation des mesures potentiométriques au moyen des courbes de polarisation. *Anal. Chim. Acta* **1952**, *7*, 77–94. [[CrossRef](#)]
4. Bancroft, W.D. Anode reactions. *Trans. Electrochem. Soc.* **1937**, *33*, 195–205. [[CrossRef](#)]
5. Bard, A.J. (Ed.) *Encyclopedia of Electrochemistry of the Elements*; Marcel Dekker, Inc.: New York, NY, USA, 1975; Volume IV, Chapter 6; p. 275. ISBN 0-8247-2504-2.
6. Bouroushian, M. *Electrochemistry of Metal Chalcogenides*; Springer: Heidelberg/Berlin, Germany, 2010.
7. Dribinskii, A.V.; Tarasevich, M.R.; Kazarinov, V.E. Electrocatalysis on carbon materials. *Mater. Chem. Phys.* **1989**, *22*, 377–400. [[CrossRef](#)]
8. Hunger, T.; Lapicque, F.; Storck, A. Electrochemical oxidation of sulphite ions at graphite electrodes. *J. Appl. Electrochem.* **1991**, *21*, 588–596. [[CrossRef](#)]
9. Sun, H.Q.; Liu, S.Z.; Zhou, G.L.; Ang, H.M.; Tade, M.O.; Wang, S.B. Reduced graphene oxide for catalytic oxidation of aqueous organic pollutants. *ACS Appl. Mater. Interfaces* **2012**, *4*, 5466–5471. [[CrossRef](#)]
10. Kong, X.K.; Chen, C.L.; Chen, Q.W. Doped graphene for metal-free catalysis. *Chem. Soc. Rev.* **2014**, *43*, 2841–2857. [[CrossRef](#)] [[PubMed](#)]
11. Frank, B.; Blume, R.; Rinaldi, A.; Trunschke, A.; Schlogl, R. Oxygen Insertion Catalysis by sp² Carbon. *Angew. Chem. Int. Ed.* **2011**, *50*, 10226–10230. [[CrossRef](#)]
12. Frank, B.; Zhang, J.; Blume, R.; Schlogl, R.; Su, D.S. Heteroatoms increase the selectivity in oxidative dehydrogenation reactions on nanocarbons. *Angew. Chem. Int. Ed.* **2009**, *48*, 6913–6917. [[CrossRef](#)]
13. Zhang, J.; Liu, X.; Blume, R.; Zhang, A.H.; Schlogl, R.; Su, D.S. Surface-modified carbon nanotubes catalyze oxidative dehydrogenation of n-butane. *Science* **2008**, *322*, 73–77. [[CrossRef](#)] [[PubMed](#)]
14. Oh, W.D.; Dong, Z.; Lim, T.T. Generation of sulfate radical through heterogeneous catalysis for organic contaminants removal: Current development, challenges and prospects. *Appl. Catal. B Environ.* **2016**, *194*, 169–201. [[CrossRef](#)]
15. Liu, S.Z.; Peng, W.C.; Sun, H.Q.; Wang, S.B. Physical and chemical activation of reduced graphene oxide for enhanced adsorption and catalytic oxidation. *Nanoscale* **2014**, *6*, 766–771. [[CrossRef](#)]
16. Jiang, D.E.; Sumpter, B.G.; Dai, S.J. Unique chemical reactivity of a graphene nanoribbon's zigzag edge. *Chem. Phys.* **2007**, *126*, 134701. [[CrossRef](#)]
17. Zhao, Y.; Yang, L.J.; Chen, S.; Wang, X.Z.; Ma, Y.W.; Wu, Q.; Jiang, Y.F.; Qian, W.J.; Hu, Z.J. Can boron and nitrogen co-doping improve oxygen reduction reaction activity of carbon nanotubes? *Am. Chem. Soc.* **2013**, *135*, 1201–1204. [[CrossRef](#)] [[PubMed](#)]
18. Bennett, J.E.; Gilbert, B.C.; Stell, J.K. Mechanisms of Peroxide Decomposition. EPR Studies of the One-electron Oxidation of the Peroxymonosulphate Anion (HOOSO₃[−]) and the Reactions of SO₅[−]. *J. Chem. Soc. Perkin Trans.* **1991**, *2*, 1105–1110. [[CrossRef](#)]
19. Gilbert, B.C.; Stell, J.K. Mechanisms of peroxide decomposition. An ESR study of the reactions of the peroxomonosulphate anion (HOOSO₃[−]) with Ti III, Fe II, and α-oxygen-substituted radicals. *J. Chem. Soc. Perkin Trans.* **1990**, *2*, 1281–1288. [[CrossRef](#)]
20. Gilbert, B.C.; Stell, J.K. Mechanisms of peroxide decomposition: An electron paramagnetic resonance study of the reaction of the peroxomonosulphate anion (HOOSO₃[−]) with Cu I. A marked contrast in behaviour with that of Ti^{III} and Fe^{II}. *J. Chem. Soc. Faraday Trans.* **1990**, *86*, 3261–3266. [[CrossRef](#)]
21. Bartlett, P.N. *Electrochemistry of Carbon Electrodes (Band 16) in Advances in Electrochemical Sciences and Engineering*; Richard, C., Lipkowsky, J., Eds.; Wiley-VCH: Weinheim, Germany, 2015.
22. van Veen, J.A.R.; van Baar, J.F.; Kroese, K.J. Effect of heat treatment on the performance of carbon-supported transition-metal chelates in the electrochemical reduction of oxygen. *J. Chem. Soc. Faraday Trans.* **1981**, *177*, 2827–2843. [[CrossRef](#)]
23. Gupta, S.; Tryk, D.; Bae, I.; Aldred, W.; Yeager, E. Heat-treated polyacrylonitrile based catalysts for oxygen electroreduction. *J. Appl. Electrochem.* **1989**, *19*, 19–27. [[CrossRef](#)]
24. Zhou, Y.; Neyerlin, K.; Olson, T.S.; Pylypenko, S.; Bult, J.; Dinh, H.N.; Gennett, T.; Shao, Z.; O'Hayre, R. Enhancement of Pt and Pt-alloy fuel cell catalyst activity and durability via nitrogen-modified carbon supports. *Energy Environ. Sci.* **2010**, *3*, 1437–1446. [[CrossRef](#)]
25. Pylypenko, S.; Borisevich, A.; More, K.L.; Corpuz, A.R.; Holme, T.; Dameron, A.A.; Olson, T.S.; Dinh, H.N.; Gennett, T.; O'Hayre, R. Nitrogen: Unraveling the secret to stable carbon-supported Pt-alloy electrocatalysts. *Energy Environ. Sci.* **2013**, *6*, 2957–2964. [[CrossRef](#)]

26. Titirici, M.M.; White, R.J.; Brun, N.; Budarin, V.L.; Su, D.S.; del Monte, F.; Clark, J.H.; MacLachlan, M.J. Sustainable carbon materials. *Chem. Soc. Rev.* **2015**, *44*, 250–290. [[CrossRef](#)] [[PubMed](#)]
27. Wang, H.; Maiyalagan, T.; Wang, X. Review on recent progress in nitrogendoped graphene: Synthesis, characterization, and its potential applications. *ACS Catal.* **2012**, *2*, 781–794. [[CrossRef](#)]
28. Czerw, R.; Terrones, M.; Charlier, J.C.; Blase, X.; Foley, B.; Kamalakaran, R.; Grobert, N.; Terrones, H.; Tekleab, D.; Ajayan, P.M.; et al. Identification of electron donor states in N-doped carbon nanotubes. *Nano Lett.* **2001**, *1*, 457–460. [[CrossRef](#)]
29. Wood, K.N.; O’Hayre, R.; Pylypenko, S. Recent progress on nitrogen/carbon structures designed for use in energy and sustainability applications. *Energy Environ. Sci.* **2014**, *7*, 1212–1249. [[CrossRef](#)]
30. Unni, S.M.; Dhavale, V.M.; Pillai, V.K.; Kurungot, S. High Pt Utilization Electrodes for Polymer Electrolyte Membrane Fuel Cells by Dispersing Pt Particles Formed by a Preprecipitation Method on Carbon “Polished” with Polypyrrole. *J. Phys. Chem. C* **2010**, *114*, 14654–14661. [[CrossRef](#)]
31. Olson, T.S.; Pylypenko, S.; Atanassov, P.; Asazawa, K.; Yamada, K.; Tanaka, H. Anion-Exchange Membrane Fuel Cells: Dual-Site Mechanism of Oxygen Reduction Reaction in Alkaline Media on Cobalt–Polypyrrole Electrocatalysts. *J. Phys. Chem. C* **2010**, *114*, 5049–5059. [[CrossRef](#)]
32. Ralph, T.R.; Hogarth, M.P. Catalysis for low-temperature fuel cells—Part 1: The cathode challenges. *Plat. Met. Rev.* **2002**, *46*, 4–15.
33. Wang, J.; Wang, G.; Miao, S.; Liab, J.; Bao, X. Graphene -supported iron-based nanoparticles encapsulated in nitrogen-doped carbon as a synergistic catalyst for hydrogen evolution and oxygen reduction reactions. *Faraday Discuss* **2014**, *176*, 135–151. [[CrossRef](#)]
34. Lambin, P.; Loiseau, A.; Culot, C.; Biro, L. Structure of carbon nanotubes probed by local and global probes. *Carbon* **2002**, *40*, 1635–1648. [[CrossRef](#)]
35. Walanda, D.K.; Lawrance, G.A.; Donne, S.W. Hydrothermal MnO₂: Synthesis, structure, morphology and discharge performance. *J. Power Sources* **2005**, *139*, 325–341. [[CrossRef](#)]
36. Pchelarov, G.; Uzun, D.; Razkazova-Velkova, E.; Petrov, K. Oxidation of Sulphites by Electrodes Made of Novel Materials for Use in Microbial Fuel Cells. *Biomed. J. Sci. Tech. Res.* **2020**, *26*, 20137–20140.
37. Brunauer, A.S.; Emmett, P.H.; Teller, E. Adsorption of gases in multimolecular layers. *J. Am. Chem. Soc.* **1938**, *60*, 309–319. [[CrossRef](#)]
38. Niyogi, S.; Hamon, M.N.; Hu, H.; Zhao, B.; Bhowmik, P.; Sen, R.; Itkis, M.E.; Haddon, R.C. Chemistry of single-walled carbon nanotubes. *Acc. Chem. Res.* **2002**, *35*, 1105–1113. [[CrossRef](#)]
39. Haddon, R.C.; Scuseria, G.E.; Smalley, R.E. C₂₄₀s The Most Chemically Inert Fullerene? *Chem. Phys. Lett.* **1997**, *272*, 38–42. [[CrossRef](#)]
40. Boul, P.J.; Liu, J.; Mickelson, E.T.; Huffman, C.B.; Ericson, L.M.; Chiang, I.W.; Smith, K.A.; Colbert, D.T.; Hauge, R.H.; Margrave, J.L.; et al. Reversible Sidewall Functionalization of Buckytubes. *Chem. Phys. Lett.* **1999**, *310*, 367–372. [[CrossRef](#)]
41. Zhou, H.; Han, G.; Xiao, Y.; Chang, Y.; Zhai, H.J. Facile preparation of polypyrrole/graphene oxide nanocomposites with large areal capacitance using electrochemical codeposition for supercapacitors. *J. Power Sources* **2014**, *263*, 259–267. [[CrossRef](#)]
42. Chalmers, E.; Lee, H.; Zhu, C.; Liu, X. Increasing the Conductivity and Adhesion of Polypyrrole Hydrogels with Electropolymerized Polydopamine. *Chem. Mater.* **2020**, *32*, 234–244. [[CrossRef](#)]
43. Kovtyukhova, N.I.; Mallouk, T.E.; Pan, L.; Dickey, E.C. Individual single-walled nanotubes and hydrogels made by oxidative exfoliation of carbon nanotube ropes. *J. Am. Chem. Soc.* **2003**, *125*, 9761–9769. [[CrossRef](#)]
44. Chen, X.; Wang, X.; Fang, D. A review on C1s XPS—Spectra for some kinds of carbon materials. *Fuller. Nanotub. Carbon Nanostruct.* **2020**, *28*, 1048–1058. [[CrossRef](#)]
45. Fujimoto, A.; Yamada, Y.; Koinuma, M.; Sato, S. Origins of sp³C peaks in C_{1s} X-ray Photoelectron Spectra of Carbon Materials. *Anal. Chem.* **2016**, *88*, 6110–6114. [[CrossRef](#)] [[PubMed](#)]
46. Riviere, J.P.; Cahoreau, M.; Ahoreau-Pacaud, Y. Spectroscopic studies of BN films deposited by dynamic ion mixing. *Thin Solid Film.* **1993**, *227*, 44–53. [[CrossRef](#)]
47. Poleunis, C.; Weng, L.T.; Sclavons, M.; Bertrand, P.; Franquinet, P.; Legras, R.; Carlier, V. Sizing removal and functionalization of the carbon fiber surface studied by combined TOF SIMS and XPS. *J. Adhes. Sci. Technol.* **1995**, *9*, 859–871.
48. Su, N.; Li, H.B.; Yuan, S.J.; Yi, S.P.; Yin, E.Q. Synthesis and characterization of polypyrrole doped with anionic spherical polyelectrolyte brushes. *Express Polym. Lett.* **2012**, *9*, 697–705. [[CrossRef](#)]
49. Malitesta, C.; Losito, I.; Sabbatini, L.; Zamboni, P.G. New findings on polypyrrole chemical structure by XPS coupled to chemical derivatization labelling. *J. Electron. Spectrosc. Relat. Phenom.* **1995**, *76*, 629–634. [[CrossRef](#)]
50. Biesinger, M.C.; Payne, B.P.; Grosvenor, A.P.; Lau, L.W.M.; Gerson, A.R.; Smart, R.S.C. Resolving surface chemical states in XPS analysis of first row transition metals, oxides and hydroxides: Cr, Mn, Fe, Co and Ni. *Appl. Surf. Sci.* **2011**, *257*, 2717–2730. [[CrossRef](#)]
51. Koleva, V.; Boyadzhieva, T.; Zhecheva, E.; Nihtianova, D.; Simova, S.; Tyuliev, G.; Stoyanova, R. Precursor-based methods for low-temperature synthesis of defectless NaMnPO₄ with an olivine- and maricite-type structure. *CrystEngComm* **2013**, *15*, 9080–9089. [[CrossRef](#)]
52. Nikolova, V.; Iliev, P.; Petrov, K.; Vitanov, T.; Zhecheva, E.; Stoyanova, R.; Valov, I.; Stoychev, D. Electrocatalysts for bifunctional oxygen/air electrodes. *J. Power Sources* **2008**, *185*, 727–733. [[CrossRef](#)]
53. Atkins, P.; de Paula, J. *Physical Chemistry*, 8th ed.; W.H. Freeman and Company: New York, NY, USA, 2006; p. 939.

54. Budevski, E.B.; Iliev, I.D.; Kaisheva, A.R.; Gamburtzev, S.S.; Vakanova, E.B. Method for Producing Powdered Wetproofed Material Useful in Making Gas-Diffusion Electrodes. U.S. Patent No. 4031 033A, 1972.
55. Uzun, D.; Razkazova-Velkov, E.; Petrov, K.; Beschkov, V. Electrochemical method for energy production from hydrogen sulfide in the Black sea waters in sulfide-driven fuel cell. *BullChemComm* **2015**, *47*, 859–866.
56. Jeffry, G.H.; Bassett, J.; Mandham, J.; Denney, R.C. *Vogel's Textbook of Quantitative Chemical Analysis*, 5th ed.; Longman Scientific and Technical: New York, NY, USA, 1989; pp. 398–399.
57. Jeffery, G.H.; Bassett, J.; Mandham, J.; Denney, R.C. *Vogel's, Textbook of Quantitative Chemical Analysis*, 5th ed.; John Wiley: New York, NY, USA, 1989; p. 340.
58. Enache, A.-F.; Dan, M.L.; Vaszilcsin, N. Electrochemical Oxidation of Sulphite in Neutral Media on Platinum Anode. *Int. J. Electrochem. Sci.* **2018**, *13*, 4466–4478. [[CrossRef](#)]
59. Márquez-Montes, R.A.; Kawashima, K.; Vo, K.M.; Chávez-Flores, D.; Collins-Martínez, V.H.; Buddie Mullins, C.; Ramos-Sánchez, V.H. Simultaneous Sulfite Electrolysis and Hydrogen Production Using Ni Foam-Based Three-Dimensional Electrodes. *Environ. Sci. Technol.* **2020**, *54*, 12511–12520. [[CrossRef](#)]
60. D'Souza, F.; Choi, J.P.; Kutner, W. Electrocatalytic Dehalogenation of 1,2-Dihaloethanes by the C₆₀, C₇₀, C₇₆, C₇₈, and C₈₄ Fullerene Anions: Structure–Reactivity Aspects. *J. Phys. Chem. B* **1999**, *103*, 2892–2896. [[CrossRef](#)]
61. Shi, Z.; Zhang, J.; Liu, Z.; Wang, H.; Wilkinsn, D.P. Current status of ab initio quantum chemistry study for oxygen electroreduction on fuel cell catalysts. *Electrochim. Acta* **2006**, *51*, 1905–1916. [[CrossRef](#)]
62. Troullier, N.; Martins, J.L. Efficient pseudopotentials for plane-wave calculations. *Phys. Rev. B* **1991**, *43*, 1993–2006. [[CrossRef](#)]
63. Carroll, D.L.; Redlich, P.; Ajayan, P.M.; Charlier, J.C.; Blasé, X.; De Vita, A.; Car, R. Electronic Structure and Localized States at Carbon Nanotube Tips. *Phys. Rev. Lett.* **1997**, *78*, 2811–2814. [[CrossRef](#)]
64. Skavås, E.; Adriaens, A.; Hemmingsen, T. A Comparative Study of Sulphite Oxidation Under Alkaline Conditions by Use of Wall-jet Flow Cell and Rotating Disc Electrode. *Int. J. Electrochem. Sci.* **2006**, *1*, 414–424.